MOTION AND PARAMETER ESTIMATION FOR THE ROBOTIC CAPTURE OF A NON-COOPERATIVE SPACE TARGET CONSIDERING EGOMOTION UNCERTAINTY

Hrishik Mishra and Phillip Schmidt

Institute of Robotics and Mechatronics,
DLR (German Aerospace Center),
82234 Weßling Germany

ABSTRACT

This paper investigates an On-Orbit Servicing (OO-Servicing) estimation problem in using a robot-equipped spacecraft (On-Orbit Servicer (OOS)) for capturing a non-cooperative satellite (Target) which lacks navigation aids and whose parameters of motion, geometry and inertia may be known only with limited certainty during the initial rendezvous. The uncertainty in the robot's own pose (egomotion uncertainty) during the subsequent manipulator approach also limits the accuracy of such a Position-based Visual Servo (PBVS) capture. Vision measurements are an appealing choice but the slow sampling restricts the servoing rate and the processing delay poses a nontrivial multi-sensor estimation problem. Furthermore, they are also characterized by variable noise and a high outlier density. In this paper, an estimation scheme that facilitates such a vision-based capture with an end-effector mounted camera (eye-in-hand) is investigated. A novel Extended Kalman Filter (EKF) is implemented which robustly estimates the states and parameters by using the available measurements: the relative pose between the Target and camera, and the robot's kinematics. The proposed estimator is shown to be robust towards the aforementioned problems that are associated with vision sensors. In both phases of approach, the proposed estimator's robustness is demonstrated through simulations and Software In Loop (SIL).

Key words: Extended Kalman Filter (EKF); Position-based Visual Servo (PBVS); On-Orbit Servicing (OO-Servicing); .

1. INTRODUCTION

Deutsche Orbitale Servicing Mission (DEOS) from Deutsches Zentrum für Luft- und Raumfahrt (DLR) was pivotal in steering the narrative in On-Orbit Servicing (OO-Servicing) towards capture of non-cooperative spacecraft as mission objectives. The relative navigation in this instance was planned with a vision-based system. This specific problem of a vision-based robotic capture of a tumbling satellite is addressed in this paper. In such a scenario of OO-Servicing, an On-Orbit Servicer (OOS) must first ensure precise vision-based navigation which is one of the appealing choices for aiding Target-capture [1]. A preliminary requirement, however, is to determine the inertial and geometric properties of the Target using vision measurements. The estimation of these parameters are pivotal in the subsequent servoing process. For such a camera-aided system, an estimation scheme which uses the slow, noisy and delayed sensor data to predict the relative motion is a necessity. The primary focus of this paper is to develop features that address these unique problems and to analyze the estimator behavior through the two preliminary phases of approach: *Rendezvous* and *Manipulator*. In the former phase, the objective is to decrease the Target's parameter uncertainty while the latter phase is directed towards aiding the Position-based Visual Servo (PBVS). These two approach phases are explained in figure 1. Since, the observed motion in the camera depends on both the Target and the OOS, OOS disturbances will directly affect the PBVS performance. In this paper, a novel approach is proposed which uses the camera and the robot's kinematics to reduce the effect of such egomotion uncertainty during PBVS in the latter phase.

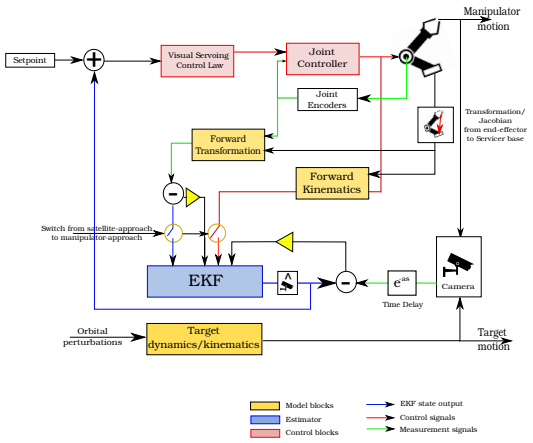

Figure 1: Block diagram of proposed Observer-based Visual Servo

Since the relative kinematics/dynamics between the Target and the OOS is nonlinear, Extended Kalman Filter (EKF) is often a suitable candidate [1]. In the context of OO-Servicing, this has been established and demonstrated in various instances [2] [3]. The treatment of this problem in [4] and [5] provide a relevant discussion in the context of estimator observability and degenerate conditions. It is worth pointing out that inertia identification using EKF requires reparametrization to avoid explicit EKF constraints. In this paper, the inertia expressions provided in [3] have been evaluated. In any case, for torque-free motion, the inertia matrix can only be determined upto a scaling factor [5].

In an estimation scheme based on vision-measurements, it is common to utilize a pre-filtering algorithm [4] which provides coarse pose measurements using a computer vision technique. Firstly, the sampling rate of such an algorithm is non-uniform and much lower than the controller. Furthermore, the measurement samples are delayed due to processing. Although an event-driven EKF will overcome the sampling problem, the processing delay poses a non-trivial estimation problem when multiple sensors are used. The mathematical foundation of such measurement updates have been found in [6] and [7]. Zhang et al. termed this situation as an Out-of-Sequence-Measurement (OOSM). Failure to account for the delay will obviously lead to large errors. Secondly, the measurement error characteristics are sensitive to bad lighting conditions and occlusion [3]. Additionally, the noise characteristics of vision algorithms are not strictly Gaussian [8]. So, it is a natural estimator requirement to exhibit adaptive response to vision-based measurements. A finite memory covariance-matching technique was proposed in [3]. Among Bayesian approaches [9], methods based on Variational Bayesian (VB) have recently gained traction [10] [11]. This paper explores the VB-adaptive technique [10] and is shown to converge in only a few update iterations. Furthermore, the pre-filtering algorithm frequently reports outlier measurements which adversely affect the estimator's operating health after fusion. For outlier robustness in an estimator, the Mahalanobis distance as a discriminating function was proposed in [12]. In this paper, a threshold based on χ^2-test is used for Outlier Rejection (OR).

In the context of OO-Servicing, the relative translational motion between two bodies in orbit are given by the Clohessy-Wiltshire [13] linearized equations and have been consistently used in rendezvous and docking applications. It is natural that these along with the torque-free Euler equations are used to model relative motion dynamics between OOS and Target. The relative orientations in the EKF are modeled using multiplicative quaternion errors to avoid the quaternion covariance matrix' rank deficiency problem [14] [15] [16]. In this paper, the small rotation approximation from [16] is used.

Visual servoing has been successfully employed in terrestrial applications since 1980s, as has been surveyed by Hutchinson et al. in [17]. In contrast to terrestrial visual servoing techniques, for space applications, free-flying or free-floating kinematics/dynamics of the OOS have to be modeled. In this volume of work, the robot's configuration is defined in $SE(3)$ as the pose of the OOS mass center relative to the camera.

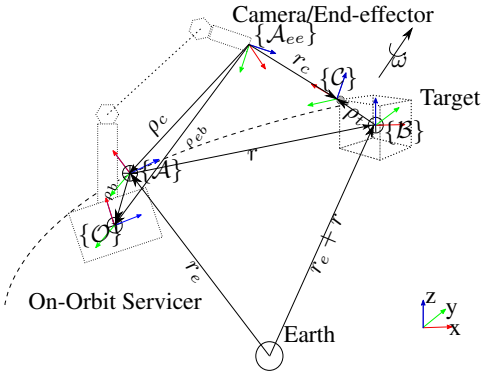

Figure 2: Body diagrams of OOS and tumbling spacecraft

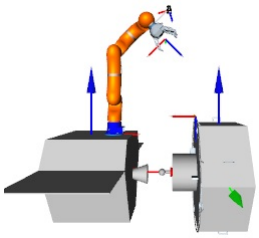

Figure 3: Simulated scenario of the grasping problem at DLR's OOS-simulator

2. DEFINING THE MODEL

As a convention, quaternions, vectors and Matrices are indicated by boldface symbols with an additional over-line ($\bar{\cdot}$), lowercase alphabet and uppercase alphabet respectively. Figure 2 is a diagrammatic representation of an OO-Servicing scenario in which an OOS is approaching the Target in a similar orbit. Frame $\{\mathcal{A}\}$ is centered at the OOS's mass center and oriented along the orbital frame. $\{\mathcal{O}\}$ is the OOS's base frame that is determined by the OOS's manipulator kinematics from the end-effector to the base. The camera is assumed to be mounted on the end-effector and the camera frame $\{\mathcal{A}_{ee}\}$ has its z-axis perpendicular to the image plane, x-axis to the right of image center and the y-axis completing the triad. $\{\mathcal{A}\}$ is located at a position of $\boldsymbol{\rho}_c$ from $\{\mathcal{A}_{ee}\}$ and its orientation is denoted by a quaternion $\bar{\Im}$. Following the conventional models [3] [4], the Target body frame $\{\mathcal{B}\}$ is the oriented parallel to the principal axes of inertia and is centered at the mass center of the Target. The feature/grasping plane (marked by grey) that is visible to the camera lies in $\{\mathcal{C}\}$ at the feature center. The relative pose of the grasping frame $\{\mathcal{C}\}$ with respect to body frame $\{\mathcal{B}\}$ is given by position $\boldsymbol{\rho}_t$ and an orientation quaternion $\bar{\boldsymbol{\eta}}$. The Target is assumed to be have to torque-free motion in space characterized by an angular velocity $\boldsymbol{\omega}$ expressed with respect to $\{\mathcal{A}\}$ in the Target body frame. Moreover, $\{\mathcal{A}\}$ is the orbital reference frame and can be assumed for a short duration

to be inertial during visual servoing. The Target has a relative position $\boldsymbol{r}$ and an orientation quaternion $\bar{\boldsymbol{q}}$ with respect to $\{\mathcal{A}\}$. One of the primary advantages of this representation is the decoupling of translational and rotational dynamics [2], [3] of the Target. This also simplifies the quaternion calculations since the error dynamics for $\bar{\boldsymbol{q}}$ and $\bar{\boldsymbol{\eta}}$ are expressed in the Target's body frame. This aspect will become clear once the attitude error dynamics are derived in section 3.1.

The robot pose uncertainty is a contributing factor only during the *Manipulator*-approach. In this phase, however, the translational dynamics due to orbital motion do not have a contribution.

3. DERIVING THE MODEL

3.1. Attitude in Multiplicative EKF (MEKF)

In this paper, the attitude of one frame with respect to another is expressed using $\mathbb{R}^4$ magnitude-constrained quaternions like. The time-derivative of the quaternion $\bar{\boldsymbol{q}}$ with respect to the relative-frame is related to the angular velocity $\boldsymbol{\omega}$ (in body frame) as given by,

$$\dot{\bar{\boldsymbol{q}}}(t) = \frac{1}{2}\bar{\boldsymbol{\omega}} \otimes \bar{\boldsymbol{q}}(t) \tag{1a}$$

where $\bar{\boldsymbol{\omega}}$ is simply $\begin{bmatrix}\boldsymbol{\omega}(t)\\ 0\end{bmatrix}$.

Applying the differential equation above to the current problem, $\boldsymbol{\omega}$ is the angular velocity of the Target with respect to $\{\mathcal{A}\}$ in the Target's body frame.

The reader is referred to detailed properties and derivations of quaternions in [18] and [19].

Since a quaternion is constrained in magnitude and has 3 Degrees of Freedom (DOF), the vector components are not statistically independent which results in singular covariance matrix for a full-state quaternion [16]. Instead of the full-state quaternion, it is common to estimate an unconstrained 3-dimensional attitude vector in a EKF, $\boldsymbol{a}$. From this vector, an orientation error quaternion $\delta\bar{\boldsymbol{q}}$ is estimated which can be used to express the estimated attitude, $\hat{\bar{\boldsymbol{q}}}$. For small error rotation about the angular axis, $\delta\theta$, the differential quaternion can be written as,

$$\delta\bar{\boldsymbol{q}} \approx \begin{bmatrix}\frac{1}{2}\delta\boldsymbol{\theta}\\ 1\end{bmatrix} \Rightarrow \delta\bar{\boldsymbol{q}} = \delta\bar{\boldsymbol{q}}(\delta\boldsymbol{\theta}) \tag{1ba}$$

In this small-angle formulation, $\boldsymbol{a} = \delta\boldsymbol{\theta}$. Some authors [3] use an alternative notation, $\boldsymbol{a} = \frac{1}{2}\delta\boldsymbol{\theta}$.

MEKF is the formulation in which the orientation quaternion estimate, $\hat{\bar{\boldsymbol{q}}}$ is derived as a product of the quaternions representing error $\delta\bar{\boldsymbol{q}}$ and the reference erroneous attitude $\bar{\boldsymbol{q}}_{ref}$ [14]. There are two ways to formulate the error quaternion, $\delta\bar{\boldsymbol{q}}$.

$$\delta\bar{\boldsymbol{q}}_b(\boldsymbol{a}_b) = \bar{\boldsymbol{q}} \otimes \bar{\boldsymbol{q}}^*_{ref} \tag{1c}$$

$$\delta\bar{\boldsymbol{q}}_i(\boldsymbol{a}_i) = \bar{\boldsymbol{q}}^*_{ref} \otimes \bar{\boldsymbol{q}} \tag{1d}$$

where (1c) expresses the attitude error in the body frame while (1d) expresses the error in the relative reference frame. Details of such expressions for $\boldsymbol{a}_b$ and their corresponding dynamics can be derived using the mathematical basis provided in [14], [15] and [16]. The error vector $\dot{\boldsymbol{a}_b}$ dynamics have also been defined in [3, see App. A], where the expression differs from that of the previous authors only by a factor of 2. The attitude error dynamics can be written according to [3] as,

$$\dot{\boldsymbol{a}}_b = f_a(\boldsymbol{a}_b, \delta\boldsymbol{\omega}) \approx -\hat{\boldsymbol{\omega}} \times \boldsymbol{a}_b + \frac{1}{2}\delta\boldsymbol{\omega} \tag{1e}$$

where $\hat{\boldsymbol{\omega}}$ is piece-wise constant. In [20], the authors have made a comparative study on the choice of reference frames and derived the dynamics for both formulations (1c) and (1d). Pertinent to the discussion here, for the error expression in the relative frame, eq. (1d), $\dot{\boldsymbol{a}}_i = \boldsymbol{0}$.

In estimation, the attitude error in body frame is favorable to estimate angular velocity due to the presence of $\delta\boldsymbol{\omega}$ in its dynamics. In the relative frame, however, attitude estimation is the only mathematical possibility.

Let us assume a nominal reference $\bar{\boldsymbol{q}}_r$, error quaternions, $\delta\bar{\boldsymbol{q}}_{(.)}$ and the true attitude being $\bar{\boldsymbol{q}}$. Performing quaternion multiplication according to (1d) and (1c), we obtain the vector($\boldsymbol{q}_{(.)}$) and scalar components($q_{(.)}$). Ignoring the identical scalar components and rearranging the vector parts and equating both the resultant equations, we get, $\delta\boldsymbol{q}_b - \lceil\boldsymbol{q}\rceil\boldsymbol{q}_r = \delta\boldsymbol{q}_i - \lceil\boldsymbol{q_r}\rceil\boldsymbol{q}$. Solving this equation, we get,

$$\begin{aligned}
\delta\boldsymbol{q}_i =& \delta\boldsymbol{q}_b + 2\lceil\boldsymbol{q_r}\rceil\boldsymbol{q}\\
=& \delta\boldsymbol{q}_b + 2\lceil\boldsymbol{q_r}\rceil\left[\delta\bar{\boldsymbol{q}} \otimes \bar{\boldsymbol{q}}_r\right]_v\\
=& \delta\boldsymbol{q}_b + 2\lceil\boldsymbol{q_r}\rceil(-\lceil\boldsymbol{\delta q_b}\rceil\boldsymbol{q}_r + \delta q_b\boldsymbol{q}_r + q_r\delta\boldsymbol{q}_b)\\
=& \delta\boldsymbol{q}_b + (-2\lceil\boldsymbol{q_r}\rceil\lceil\boldsymbol{\delta q_b}\rceil\boldsymbol{q}_b) + (2\delta q\lceil\boldsymbol{q_r}\rceil\boldsymbol{q_r}) + (2q_r\lceil\boldsymbol{q_r}\rceil\delta\boldsymbol{q})\\
=& (\boldsymbol{I} + 2\lceil\boldsymbol{q_r}\rceil^2 + 2q_r\lceil\boldsymbol{q_r}\rceil)\delta\boldsymbol{q}\\
=& (\boldsymbol{I} + 2\boldsymbol{q}_r\boldsymbol{q}_r^T - 2||\boldsymbol{q}_r||^2\boldsymbol{I} + 2q_r\boldsymbol{q}_r)\delta\boldsymbol{q}_b\\
=& ((2q_r - 1)\boldsymbol{I} + 2\boldsymbol{q}_r\boldsymbol{q}_r^T + 2q_r\lceil\boldsymbol{q_r}\rceil)\delta\boldsymbol{q}_b
\end{aligned}$$

$$\Rightarrow \delta\boldsymbol{q}_i = \boldsymbol{R}(\bar{\boldsymbol{q}}_r)\delta\boldsymbol{q}_b \tag{1f}$$

which defines the relationship between quaternion errors in involved frames. The Target's orientation, $\bar{\boldsymbol{q}}$ is expressed in the body frame $\{\mathcal{B}\}$ in terms of its error dynamics as shown in (1e)

3.2. Attitude Dynamics

Following the authors in [3], the rotational dynamics are expressed in terms of inertial ratios $\boldsymbol{p}$ by modifying the Newton-Euler equations for torque-free motion. [3, see App. B]

$$\dot{\boldsymbol{\omega}} = \boldsymbol{\psi}(\boldsymbol{p}, \boldsymbol{\omega}) + \mathbf{J}(\boldsymbol{p})\epsilon_\tau \tag{3a}$$

where $\boldsymbol{p} = \begin{bmatrix} \frac{I_{yy}-I_{zz}}{I_{xx}} \\ \frac{I_{zz}-I_{xx}}{I_{yy}} \\ \frac{I_{xx}-I_{yy}}{I_{zz}} \end{bmatrix}$ is the inertia reparametrization and rest of the symbols in (3a) are in keeping with the equations provided in [3].

Linearizing about a nominal state-space point, $\underline{\boldsymbol{\omega}}$ and $\underline{\boldsymbol{p}}$ gives,

$$\frac{d}{dt}\delta\boldsymbol{\omega} = \mathbf{M}(\underline{\boldsymbol{\omega}}, \underline{\boldsymbol{p}})\delta\boldsymbol{\omega} + \mathbf{N}(\underline{\boldsymbol{\omega}})\delta\boldsymbol{p} + \mathbf{J}(\boldsymbol{p})\epsilon_\tau \tag{3b}$$

The inertial parameters are given as unchanging states,

$$\dot{\boldsymbol{p}} = \mathbf{0} \tag{3c}$$

3.3. Translational motion

The linear time-evolution of relative position between two bodies around a central body is given by the Hill-Clohessy-Wiltshire (HCW) equations [13]. Under the relevant assumptions, the HCW equations give closed-form solutions for relative position of a follower (Target) with respect to leader (OOS). In figure 2, $\{\mathcal{A}\}$ is the defined Hill frame and the solution for $\ddot{\boldsymbol{r}}$ components are are given as,

$$\ddot{\boldsymbol{r}} = HCW(\boldsymbol{r}, \dot{\boldsymbol{r}}, n) \tag{3d}$$

where, HCW is the linear function [13], n is the mean motion of the OOS in orbit. It is important to point out that $\{\mathcal{A}\}$ is not perturbed by a change in robot configuration for freefloating dynamics.

3.4. Target geometry

As mentioned in section 1, a pre-filtering algorithm is used to convert image measurements to pose measurements. In a typical scenario, the Target's geometrical and inertia parameters are uncertain or unknown. The dynamics of the grasping point pose are unchanging in time and hence the time-derivatives of pose states, $\vec{x}_\theta = \begin{bmatrix}\boldsymbol{\rho}_t^T & \delta\boldsymbol{\eta}^T\end{bmatrix}^T$ is given by,

$$\dot{\vec{x}}_\theta = \mathbf{0} \tag{4a}$$

where $\delta\boldsymbol{\eta} = \delta\bar{\boldsymbol{\eta}}_v$, $\delta\bar{\boldsymbol{\eta}} = \bar{\boldsymbol{\eta}}^*_{ref} \otimes \bar{\boldsymbol{\eta}}_k$. It is important to point out that the error-quaternion $\delta\boldsymbol{\eta}$ is expressed in the relative frame, that is, in the Target's body frame $\{\mathcal{B}\}$.

3.5. Robot pose

The pose of the robot is determined by $\boldsymbol{\rho}_c$ and the quaternion $\bar{\ni}$, and is a function of the joint angles $\boldsymbol{\phi}$. The differential kinematics of the mass center $\{\mathcal{A}\}$, as referenced from the camera frame $\{\mathcal{A}_{ee}\}$ is given by an analytic Jacobian transformation.

$$\begin{bmatrix}\dot{\boldsymbol{\rho}}_c \\ \boldsymbol{\omega}_b\end{bmatrix} = \boldsymbol{u} = \boldsymbol{J}_s(\boldsymbol{\theta})\dot{\boldsymbol{\theta}} + \boldsymbol{w}_{rob} \tag{5a}$$

where $\mathbb{E}[\boldsymbol{w}_r\boldsymbol{w}_r^T] = \boldsymbol{Q}_{rob}$ is the robot's differential kinematics disturbance covariance and accounts for egomotion uncertainty, and $\boldsymbol{\theta}$ is the joint space position vector.

As explained in 3.1, the quaternion error dynamics is rewritten in the the body frame $\{\mathcal{O}\}$ as

$$\delta\dot{\ni} = -\hat{\boldsymbol{\omega}}_b \times \ni \tag{5b}$$

Based on the phase of approach, the state-space definitions for system $\boldsymbol{\Sigma}$ can be set as follows.

$$\boldsymbol{\Sigma}_1 : \vec{\mathcal{X}} = \begin{bmatrix}\bar{\boldsymbol{q}}^T & \boldsymbol{\omega}^T & \boldsymbol{p}^T & \boldsymbol{r}^T & \dot{\boldsymbol{r}}^T & \boldsymbol{\rho}_t^T & \bar{\boldsymbol{\eta}}^T\end{bmatrix}^T \tag{5c}$$

$$\boldsymbol{\Sigma}_2 : \vec{\mathcal{X}} = \begin{bmatrix}\bar{\boldsymbol{q}}^T & \boldsymbol{\omega}^T & \boldsymbol{r}^T & \dot{\boldsymbol{r}}^T & \boldsymbol{\rho}_c{}^T & \bar{\ni}^T\end{bmatrix}^T \tag{5d}$$

whose dynamics are given by equations in (1e), (3a), (3c), (3d), (4a), (5a). The reader must also keep in mind that eq. (5c) is applicable to the *Rendezvous* while eq. (5d) is used for *Manipulator* (PBVS), among the two approach phases. In all the state-definitions above, the quaternion attitude is maintained in the 3-dimensional error form.

4. MEASUREMENT MODEL

The first measurement comprises of pose-estimates $\begin{bmatrix}\boldsymbol{r}_c^T & \bar{\boldsymbol{\mu}}^T\end{bmatrix}^T$ of the grasping frame $\{\mathcal{C}\}$, from a camera ($\{\mathcal{A}_{ee}\}$) which is mounted on the end-effector as shown in figure 3. The OOS at DLR uses a redundant monocular odometry system based on Computer-Aided Design (CAD) model. The robot pose measurements are given by forward kinematics as $\begin{bmatrix}\boldsymbol{\rho}_c{}^T & \bar{\ni}^T\end{bmatrix}^T$. So, the output function is described as,

$$y : \begin{Bmatrix}\begin{bmatrix}\boldsymbol{r}_{c_d} \\ \bar{\boldsymbol{\mu}}_d \\ \boldsymbol{\rho}_{ck} \\ \bar{\ni}_k\end{bmatrix} = \begin{bmatrix}\boldsymbol{\rho}_{c_d} + \boldsymbol{R}(\bar{\ni}_d)(\boldsymbol{r}_d + \boldsymbol{R}(\bar{\boldsymbol{q}}_d)\boldsymbol{\rho}_{t_d}) \\ \bar{\boldsymbol{\eta}}_d \otimes \bar{\boldsymbol{q}}_d \otimes \bar{\ni}_d \\ \boldsymbol{\rho}_{ck} \\ \bar{\ni}_k\end{bmatrix}\end{Bmatrix} \tag{6}$$

where $\boldsymbol{\rho}_t$ is expressed in the Target body frame $\{\mathcal{B}\}$ and k and d refer to time indices. It is clear that the camera measurements are expressions of a past state at time d.

During *Rendezvous* approach, we rewrite the relevant observation equations for camera in terms of noisy measure-

ments as,

$$\boldsymbol{y}_k(\breve{\boldsymbol{r}}_{c_k}, \breve{\bar{\boldsymbol{\mu}}}_k, \breve{\boldsymbol{\rho}}_{c_k}, \breve{\bar{\exists}}_k) = \begin{bmatrix} \boldsymbol{R}(\breve{\bar{\exists}}_d)^T(\breve{\boldsymbol{r}}_{c_k} - \breve{\boldsymbol{\rho}}_{cd}) \\ (\bar{\boldsymbol{\eta}}^*_{r_k} \otimes \breve{\bar{\boldsymbol{\mu}}}_d \otimes \breve{\bar{\exists}}^*_k \otimes \bar{\boldsymbol{q}}^*_{r_k})_v \end{bmatrix} \tag{7}$$

$$\Rightarrow \boldsymbol{h}_k(\vec{\mathcal{X}}) \doteq \begin{bmatrix} \boldsymbol{r}_d + \boldsymbol{R}(\bar{\boldsymbol{q}}_d)\boldsymbol{\rho}_{t_d} \\ (\delta\bar{\boldsymbol{q}}_d \otimes \delta\bar{\boldsymbol{\eta}}_d)_v \end{bmatrix} \tag{8}$$

It is important to point out that, as described in 3.1, the quaternion error expressions $\delta\bar{\boldsymbol{q}}$ and $\delta\bar{\boldsymbol{\eta}}$, both, are expressed in the Target's body frame, $\{\mathcal{B}\}$ and hence $\otimes$ operation is natural.

In the *Manipulator* approach, the joint angles can be used to determine the robot $SE(3)$ configuration and can be used as follows,

$$\boldsymbol{y}_k(\breve{\boldsymbol{r}}_{c_k}, \breve{\bar{\boldsymbol{\mu}}}_k, \breve{\boldsymbol{\rho}}_{c_k}, \breve{\bar{\exists}}_k) = \begin{bmatrix} \boldsymbol{\rho}_{c_d} + \boldsymbol{R}(\bar{\exists}_d)(\boldsymbol{r}_d + \boldsymbol{R}(\bar{\boldsymbol{q}}_d)\boldsymbol{\rho}_{t_d}) \\ (\bar{\boldsymbol{q}}^*_{r_d} \otimes \bar{\boldsymbol{\eta}}^* \otimes \breve{\bar{\boldsymbol{\mu}}}_d \otimes \bar{\exists}^*_{r_d})_v \\ \boldsymbol{\rho}_{c_k} \\ (\bar{\exists}_k \otimes \bar{\exists}^*_{r_k})_v \end{bmatrix} \tag{9}$$

In the above equation, let us take the camera pose quaternion error at time k, $\delta\bar{\boldsymbol{\mu}}$

$$\delta\bar{\boldsymbol{\mu}} = (\bar{\boldsymbol{q}}^*_{r_k} \otimes \bar{\boldsymbol{\eta}}^* \otimes \breve{\bar{\boldsymbol{\mu}}}_k \otimes \bar{\exists}^*_{r_k})_v \tag{10}$$

Using the quaternion expression for $\bar{\boldsymbol{\mu}}$ in (6) and substituting in (10), we get for a given time-step,

$$\delta\bar{\boldsymbol{\mu}} = (\bar{\boldsymbol{q}}^*_{r_k} \otimes \bar{\boldsymbol{\eta}}^* \otimes \bar{\boldsymbol{\eta}}_k \otimes \bar{\boldsymbol{q}}_k \otimes \bar{\exists}_k \otimes \bar{\exists}^*_{r_k})_v \tag{11}$$

$$= (\delta\bar{\boldsymbol{q}}_{i_k} \otimes \delta\bar{\exists}_k)_v \tag{12}$$

From the state-space definition in eq. (5d), $\delta\bar{\boldsymbol{q}}_v$ is expressed in $\{\mathcal{B}\}$ while $\delta\bar{\exists}_v$ is expressed in $\{\mathcal{A}\}$. In this case, $\otimes$ operation is not meaningful. In the equation above, $\delta\bar{\boldsymbol{q}}_{i_k}$ is the error quaternion in the relative frame, or the OOS's mass center frame, $\{\mathcal{A}\}$. Based on the derivation in (1f), $\delta\bar{\boldsymbol{q}}_v$ is transformed to the $\{\mathcal{A}\}$. For the sake of $\boldsymbol{\omega}$ estimation, $\delta\bar{\boldsymbol{q}}$ is propagated in $\{\mathcal{B}\}$, as discussed in section 3.1. We use this formulation to define $\boldsymbol{h}_k$ as follows.

$$\boldsymbol{h}_k(\vec{\mathcal{X}}) = \begin{bmatrix} \boldsymbol{\rho}_{c_d} + \boldsymbol{R}(\bar{\exists}_d)(\boldsymbol{r}_d + \boldsymbol{R}(\bar{\boldsymbol{q}}_d)\boldsymbol{\rho}_{t_d}) \\ (\delta\bar{\boldsymbol{q}}_{i_d} \otimes \delta\bar{\exists}_d)_v \\ \boldsymbol{\rho}_{c_k} \\ \delta(\bar{\exists}_k)_v \end{bmatrix} \tag{13}$$

where, $\delta\boldsymbol{q}_{i_k} = \boldsymbol{R}(\bar{\boldsymbol{q}}_{r_k})\delta\boldsymbol{q}_k$ and $\delta\boldsymbol{q}_k$ has been propagated by the EKF. To find the corresponding error quaternion $\delta\bar{\boldsymbol{q}}$ from the 3-dimensional form, $\delta\boldsymbol{q}$, the unity constraint is used to determine the scalar component. After convergence of the EKF, $\delta q \approx 1$. In the equations above, all $(.)_k$ represent a quantity that is computed based on a current state, $(\breve{.})$ are noisy data, the $(\bar{.})_r$ represent the computed reference quaternions and $(\bar{.})_v$ is the vector component of the quaternion.

5. KALMAN FILTER

A detailed derivation of the EKF is provided in [21] and the final equations relevant for this paper are,

Predict:

$$\begin{aligned} \hat{\boldsymbol{x}}(k+1|k) &= \boldsymbol{f_k}(\hat{\boldsymbol{x}}(k|k)) \\ \boldsymbol{\Sigma}(k+1|k) &= \boldsymbol{F}_k\boldsymbol{\Sigma}(k|k)\boldsymbol{F}_k^T + \boldsymbol{Q}_k \end{aligned} \tag{14}$$

Update:

$$\begin{aligned} \hat{\boldsymbol{x}}(k|k) &= \hat{\boldsymbol{x}}(k|k-1) + \boldsymbol{K}_k(\boldsymbol{y}_k - \boldsymbol{H}_k\hat{\boldsymbol{x}}(k|k-1)) \\ \boldsymbol{\Sigma}(k|k) &= (\mathbb{I}_{n,n} - \boldsymbol{K}_k\boldsymbol{H}_k)\boldsymbol{\Sigma}(k|k-1) \\ \boldsymbol{K}_k &= \boldsymbol{\Sigma}(k|k)\boldsymbol{H}_k^T\Big(\boldsymbol{H}_k\boldsymbol{\Sigma}(k|k-1)\boldsymbol{H}_k^T + \boldsymbol{R}_k\Big)^- \end{aligned} \tag{15}$$

where, $\boldsymbol{F}_k$ and $\boldsymbol{H}_k$ are the jacobians computed at current estimate and $\boldsymbol{x}_0 \equiv \mathcal{N}[\hat{\boldsymbol{x}}(0|0), \Sigma(0|0)]$.

6. VARIATIONAL BAYESIAN ADAPTIVE FILTERING

The non-uniformity of measurement noise characteristics $\boldsymbol{R}_k$ observed on OOS at DLR prompted the motivation to develop an EKF which exhibits adaptive response. In [9], Mehra for the first time presented a classification of such adaptive methods. In contrast to [3], a *Bayesian approach* [9] is employed in this paper and evaluated for changing noise covariances. VB inferencing is an approximate method that is used to express the posterior distribution in a tractable manner for a Bayesian approach. For the purpose of Kalman filtering [22], it is known that the posterior of the state has to be Gaussian for the assumptions to hold true. As early as 1970, in [9], the approach to estimate $\boldsymbol{R}_k$ using an Inverse-Gamma ($\boldsymbol{\Gamma}^-$) distribution was already discussed. In [10], a $\boldsymbol{\Gamma}^-$ distribution is assumed on the diagonal elements of the measurement noise covariance matrix and the equations are derived for a linear system. This methodology is employed here for adapting the measurement noise covariance for the linearized system. The derivation of the relevant equations are intuitive and the main advantage of this method is swift convergence through a few iterative update steps which start at Algorithm 1, line 5. There are three parameters in the VB-EKF: β and α determine the diagonal elements of $\hat{\boldsymbol{R}}$ while ρ is the propagation factor for the ($\boldsymbol{\Gamma}^-$) distribution. This means, if $\rho = 0.99$, adaptive response will be sluggish while $\rho = 0.1$ will make the filter sensitive.

7. OUT-OF-SEQUENCE-MEASUREMENT

The requirement is to perform multiple-sensor estimation using measurements defined in section 4. This estimation problem of processing delay in camera measurements is non-trivial and has been discussed in [7] and [6]. In the following paper, the Global Optimal update for Algorithm-I provided in [7] has been used because of

Algorithm 1 VB-EKF for each update

$\left[\hat{\boldsymbol{x}}(k+1|k), \quad \boldsymbol{\Sigma}(k+1|k)\right] \leftarrow$ `EKF-predict`$(\boldsymbol{\Sigma}(k|k), \boldsymbol{Q}_k, \hat{\boldsymbol{x}}(k|k))$ ▷ Predict:
$\hat{\alpha}_{k+1,i} \leftarrow \rho_i \alpha_{k,i} \quad \forall\, i \in \begin{bmatrix}1 & d\end{bmatrix}$
$\hat{\beta}_{k+1,i} \leftarrow \rho_i \beta_{k,i} \quad \forall\, i \in \begin{bmatrix}1 & d\end{bmatrix}$
if $\boldsymbol{y}_k \neq NULL$ **then** ▷ Update:
  for n $\leftarrow$ 1 to N **do**
    $\hat{\boldsymbol{R}}^n_{k+1} \leftarrow diag[\frac{\beta^n_{k,1}}{\alpha^n_{k,1}} ... \frac{\beta^n_{k,d}}{\alpha^n_{k,d}}]$
    $\left[\hat{\boldsymbol{x}}_n(k+1|k+1), \quad \boldsymbol{\Sigma}_n(k+1|k+1)\right] \leftarrow$ `EKF-update`$(\hat{\boldsymbol{R}}^n_{k+1}, \boldsymbol{\Sigma}(k+1|k), \hat{\boldsymbol{x}}(k+1|k))$
    $\beta^n_{k+1,i} \leftarrow \hat{\beta}_{k+1,i} + \frac{1}{2}(\boldsymbol{y}_k - \boldsymbol{h}(\hat{\boldsymbol{x}}_n(k+1|k+1))^2_i + \frac{1}{2}(\boldsymbol{H}_{k+1}\boldsymbol{\Sigma}(k+1|k+1)\boldsymbol{H}^T_{k+1})_{ii} \quad \forall\, i \in \begin{bmatrix}1 & d\end{bmatrix}$
  end for
  Set $\hat{\beta}_{k+1,i} \leftarrow \beta^N_{k+1,i}$, $\hat{\boldsymbol{x}}(k+1|k+1) \leftarrow \hat{\boldsymbol{x}}_N(k+1|k+1)$, $\boldsymbol{\Sigma}(k+1|k+1) \leftarrow \boldsymbol{\Sigma}_n(k+1|k+1)$
end if

its compact data storage. The pseudo-code for this algorithm is given in Algorithm 2. The `cam_trig` and `meas_trig` triggers are related to the time of image capture and time at which measurement is reported. The `concat` function concatenates the camera pose samples to the measurements and the OOSM-data to the current state details. The derivations of the relevant equations in [7] for this particular case is straightforward. In the algorithm 2, three additional variables apart from the conventional $\{\hat{\boldsymbol{x}}(k|k), \boldsymbol{\Sigma}(k|k)\}$ are added which are propagated through time $\{\boldsymbol{U}_{k,d}, \hat{\boldsymbol{x}}(d|k), \boldsymbol{\Sigma}(d|k)\}$, where $\hat{\boldsymbol{x}}(d|k)$ and $\boldsymbol{\Sigma}(d|k)$ are the smoothed state belief while $\boldsymbol{U}_{k,d}$ captures the correlation matrix between states at different time indices.

Algorithm 2 OOSM-EKF for each update

$\left[\hat{\boldsymbol{x}}(k+1|k), \quad \boldsymbol{\Sigma}(k+1|k)\right] \leftarrow$ `EKF-predict`$(\boldsymbol{\Sigma}(k|k), \boldsymbol{Q}_k, \hat{\boldsymbol{x}}(k|k))$ ▷ Predict:
if received(`cam_trig`) **then** ▷ OOSM init:
  $\left[\boldsymbol{U}(d|k), \hat{\boldsymbol{x}}(d|k), \boldsymbol{\Sigma}(d|k)\right]$ `oosm_init`$(\hat{\boldsymbol{x}}(k|k), \boldsymbol{\Sigma}(k|k)))$
  `oosm_flag` $\leftarrow$ `true`
end if
if $\boldsymbol{y}_k \neq NULL$ **then** ▷ Update:
  if received(`meas_trig`) **then**
    `concat`$(\boldsymbol{y}_k, \boldsymbol{H}_{k+1}, \hat{\boldsymbol{x}}(k+1|k), \boldsymbol{\Sigma}(k+1|k))$ using `OOSM` $\{\boldsymbol{U}_{k,d}, \hat{\boldsymbol{x}}(d|k), \boldsymbol{\Sigma}(d|k)\}$
    `oosm_flag` $\leftarrow$ `false`
  end if
  $\left[\hat{\boldsymbol{x}}(k+1|k+1), \quad \boldsymbol{\Sigma}(k+1|k+1)\right] \leftarrow$ `EKF-update`$(\boldsymbol{\Sigma}(k+1|k), \hat{\boldsymbol{x}}(k+1|k))$
  if `oosm_flag` is `true` **then**
    $\left[\hat{\boldsymbol{x}}(d|k+1), \quad \boldsymbol{\Sigma}(d|k+1), \quad \boldsymbol{U}_{k+1,d}\right] \leftarrow$ `oosm_run`$(\hat{\boldsymbol{x}}(d|k), \boldsymbol{\Sigma}(d|k), \boldsymbol{U}_{k,d})$ ▷ OOSM running
  end if
end if

8. OUTLIER REJECTION

The EKF measurement residual $\boldsymbol{\epsilon} = \boldsymbol{y}_k - \boldsymbol{h}(\hat{\boldsymbol{x}}(k+1|k))$ has a property that its squared Mahalanobis distance ($\boldsymbol{d}^2(\boldsymbol{\epsilon})$) has a χ^2-distribution. This property was exploited in [12] for manipulating $\boldsymbol{R}_k$ to achieve robustness. In order to avoid tampering with $\boldsymbol{R}_k$ which is set by the adaptive VB-EKF, a threshold-based OR scheme is implemented based on the χ^2-test. Henceforth, this implementation would be known as VB-OR-EKF.

9. SIMULATIONS AND SOFTWARE IN LOOP

For the purpose of evaluation, the Target, camera and orbital parameters were chosen from [3] for the simulations and Software In Loop (SIL). The estimator's performance and robustness analysis have been covered in two parts: simulations and SIL. Firstly, the estimator which is addressed as VB-OR-EKF, was implemented to facilitate VB-adaptive response and OR. Robustness has been evaluated using `MATLAB`-based simulations for surmounting vision-sensor issues that were previously discussed in 1. The simulations were used to estimate states of $\boldsymbol{\Sigma}_1$ during the *Rendezvous* phase. In order to analyze the impact delays on multiple-sensor estimation, OOSM-EKF was implemented by using a current and a delayed instance of the same simulated vision sensor measurement. In all of these simulations, the estimator performance was evaluated using metrics which is discussed in the next paragraph. Secondly, for evaluating the estimator during *Manipulator* approach with PBVS, a SIL was implemented. This consisted of the $\boldsymbol{\Sigma}_2$ EKF-implementation in `Simulink` which was interfaced with `V-REP` as shown in figure 4. The implemented controller was the PBVS analog of the visual controller given in [23]. This part of the analysis focuses only on the evaluation of the EKF for the model $\boldsymbol{\Sigma}_2$ that uses observation model derived in the section 4. This implies that $d = k$ in the time indices that were defined in section 4.

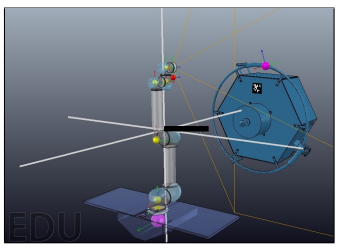

Figure 4: Virtual Robot Experimentation Platform (V-REP) scene for SIL

The Mahalanobis distance, $\boldsymbol{d}(\boldsymbol{\epsilon})$, is an indicator of the filter' current operating health and a high value is symptomatic of input uncertainty or variable measurement noise. For a normal distribution $\boldsymbol{\mathcal{X}} \equiv \mathcal{N}[\boldsymbol{\mu}, \boldsymbol{\Sigma}]$, $d^2 = (\boldsymbol{\mathcal{X}} - \boldsymbol{\mu})^T \boldsymbol{\Sigma}^- (\boldsymbol{\mathcal{X}} - \boldsymbol{\mu})$. The Cramer-Rao Bound, $\boldsymbol{CRB}$, differs from the estimator's own state error covariance, $\boldsymbol{\Sigma}(k|k)$, in that, the linearization takes

place at the true state-space. The Square Error Matrix, $\mathbf{\Pi}(k|k) = \mathbb{E}[\tilde{\boldsymbol{x}}(k|k)\tilde{\boldsymbol{x}}(k|k)^T]$ [24], is the true state error covariance. Ideally, $\mathbf{\Pi}(k|k)$ and $\mathbf{\Sigma}(k|k)$ should track the linearly varying $\boldsymbol{CRB}$ closely.

In figure 5, $\boldsymbol{d}$ has been computed for the case in which the measurement noise increases in $t \in [100, 199]$ and decreases in $t \in [200, 300]$. It is evident that the increase in $\boldsymbol{d}$ due to these changes in a conventional EKF-1 will cause large estimation errors. On the other hand, VB-EKF remains robust in this regard. The first three ($\boldsymbol{r}_c$) adapted diagonal entries in $\hat{\boldsymbol{R}}_k$ are shown in figure 6. The VB-specific parameters were set as: $\hat{\alpha}_0 = \hat{\beta}_0 = \mathbf{1}$, $N = 4$ and $\rho_i = 0.9$. The OR scheme mentioned in section 8 was implemented with a threshold, $\boldsymbol{d}^2_{th} = 50$. In figure, 7, $\boldsymbol{d}$ is peaky despite the VB-adaptive response for NO-OR, whereas, it remains unaffected for Mh-OR (VB-OR-EKF) which was implemented with the the proposed scheme. Figure 8 shows the logarithm of matrix traces discussed in the previous paragraph (9). Indices refer as follows: $1 \rightarrow$ VB-EKF, $2 \rightarrow$ EKF and $3 \rightarrow$ VB-OR-EKF. From the previous figure, it is clear that outlier density increases for $t > 250$ sec. Hence, EKF errors given by $\mathbf{\Pi}_2$ increases and is not bounded by $\boldsymbol{CRB}$. Although VB-EKF responds to the outliers by increasing $\hat{\boldsymbol{R}}_k$, a drift in $\mathbf{\Pi}_1$ implies that this is not sufficient. From this figure, it can be inferred that the proposed VB-OR-EKF is robust towards both, variable noise and outliers from the vision sensor.

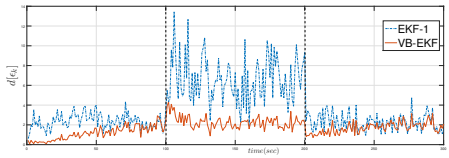

Figure 5: $\boldsymbol{d}(\boldsymbol{\epsilon})$ in presence of variable measurement noise

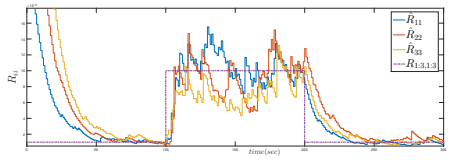

Figure 6: Diagonal entries in R_k for VB-EKF

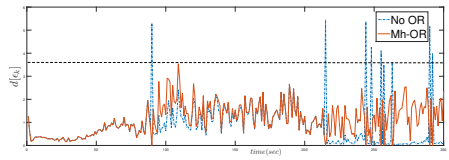

Figure 7: $\boldsymbol{d}(\boldsymbol{\epsilon})$ in presence of outliers

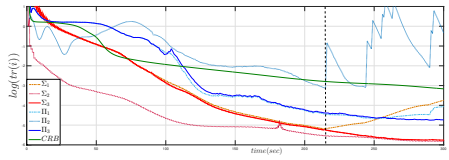

Figure 8: Matrix traces for outliers

To simulate the OOSM multiple-sensor estimation scenario, the generated vision-sensor data was sampled at $\Delta t_1 = 0.05$ sec and $\Delta t_2 = 0.1$ sec, and the latter was delayed by $\delta t_d = 0.09$ sec to account for processing delay. The Target was simulated to posses initial velocities, $\boldsymbol{\omega}_0 = [0.1125 \quad 1.5 \quad -1.1]^T$ and $\dot{\boldsymbol{r}}_0 = [0.01 \quad -0.01 \quad 0.02]^T$. The OOSM-EKF was required to optimally estimate the state using the algorithm 2 and its true state error covariance $\mathbf{\Pi}_k$ was compared to the same metric for $No - OOSM$-EKF. Figure 9 demonstrates that multiple-sensor estimation with delays can cause large tracking errors. Furthermore, in figure 10, one can verify that the estimated velocity without OOSM, $\breve{\dot{\boldsymbol{r}}}$, has an oscillatory behavior due to the delay. In contrast, the OOSM-EKF state $\hat{\dot{\boldsymbol{r}}}$ tracks the real velocities $\dot{\boldsymbol{r}}$.

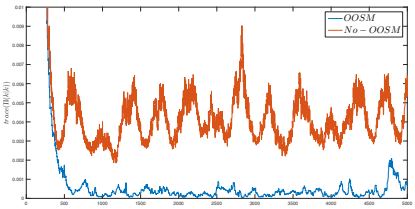

Figure 9: $\mathbf{\Pi}_k$ in presence of processing delay

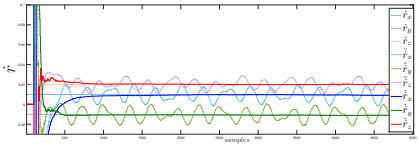

Figure 10: $\dot{\boldsymbol{r}}_k$ estimate with processing delay

In the second part of this analysis, the EKF was used as an observer for providing state-feedback during PBVS. In this sub-section, the observation model from section 4 and $\mathbf{\Sigma}_2$ define the dynamic system. The robot joints were given a joint disturbance of variance $1e^{-3}$ rad/sec while forward kinematics was simulated with error variances of $1e^{-3}$ and $1e^{-4}$ for each of the components of position and orientation respectively. The process noise and observation noise model covariance matrices for the robot have not been derived in this paper and are set to the values used for SIL. The set-point that was used for the robot end-effector was $\boldsymbol{r}_{c,d} = [0 \quad 0 \quad 1.5]^T$ relative to the tumbling Target and the estimator was allowed a convergence time of $t = 5$ sec before servoing commenced. The performance of the estimator described in [3] was compared with the one presented here. Figure 11 demonstrates that Est-1 [3] is susceptible to estimation errors because of egomotion uncertainty and robot disturbances. The EKF proposed in this paper, Est-2, takes advantage of robot's sensory information to improve estimates. Additionally, stable state estimates also imply less jerky robot behavior. This is highlighted in 12, where the PBVS [23] using state feedback from Est-1 [3], VS-1 exhibits non-smooth servoing errors. The same visual controller with Est-2 feedback, VS-2, not only produces less errors, but also achieves the control objective with a less

jerky response.

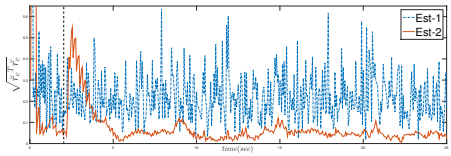

Figure 11: Estimation errors during PBVS due to egomotion uncertainty

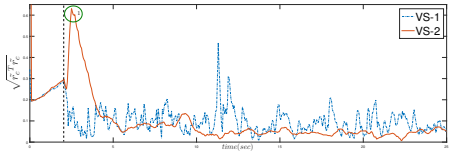

Figure 12: Visual servoing error due to egomotion uncertainty

10. CONCLUSION

This volume of work proposes a novel estimation scheme that specifically addresses the idiosyncrasies of a vision sensor, namely, processing delay, variable noise characteristics and a high outlier density. The results presented in the previous section have highlighted the impact of these issues and demonstrate the qualitative robustness of the proposed scheme with the aid of estimator performance metrics. Additionally, the proposed VB-OR-EKF is computationally efficient. VB converges in $3-4$ iterations and OOSM adds only three new variables that need to be propagated in time. A new model was presented which utilized the robot's sensory information to improve the system's state quality with an objective of using the estimator as an observer for the PBVS. Through the results obtained from a SIL implementation, it was inferred that this novel approach provides significant improvements in both estimation and PBVS. The methods explored in this paper can seamlessly extend to terrestrial PBVS applications as well. Due to the lack of modeled robot dynamics there is a large estimation error (see, figures 11 and 12) as the robot initiates servoing action at $t \approx 5$ sec. By accounting for the motion dynamics of the OOS, there is further scope for reducing estimation errors. Finally, with the strong theoretical results obtained in this paper, subsequent research naturally lends towards evaluation of the proposed estimator with data collected from the DLR-OOS.

REFERENCES

[1] Palmerini, G. B., Sabatini, M., & Gasbarri, P. 2016, in 2016 IEEE Aerospace Conference, 1–13

[2] Aghili, F. & Parsa, K. 2007, in 2007 IEEE/RSJ International Conference on Intelligent Robots and Systems, 839–846

[3] Aghili, F. & Parsa, K. 2009, JOURNAL OF GUIDANCE, CONTROL, AND DYNAMICS, 32, 538

[4] Lichter, M. D. & Dubowsky, S. 2004, in Robotics and Automation, 2004. Proceedings. ICRA '04. 2004 IEEE International Conference on, Vol. 3, 2974–2979 Vol.3

[5] Tweddle, B. E. 2013, PhD thesis, Massachusetts Institute of Technology

[6] Julier, S. J. & Uhlmann, J. K. 2005, in Proceedings of the 2005, American Control Conference, 2005., 4028–4033 vol. 6

[7] Zhang, K., Li, X. R., & Zhu, Y. 2005, IEEE Transactions on Signal Processing, 53, 1992

[8] Alcantarilla, P. & Woodford, O. 2016, Physics Letters A

[9] Mehra, R. K. 1970, in Adaptive Processes (9th) Decision and Control, 1970. 1970 IEEE Symposium on, 141–141

[10] Srkk, S. & Nummenmaa, A. 2009, IEEE Transactions on Automatic Control, 54, 596

[11] Roth, M., zkan, E., & Gustafsson, F. 2013, in 2013 IEEE International Conference on Acoustics, Speech and Signal Processing, 5770–5774

[12] Chang, G. 2014, Journal of Geodesy, 88, 391

[13] Clohessy, W. H. & Wiltshire, R. 1960, Journal of the Aerospace Sciences, 27, 653, doi: 10.2514/8.8704

[14] Landis, M. 2003, Journal of Guidance, Control, and Dynamics, 26, 311, doi: 10.2514/2.5048

[15] Landis, M. F. 2004, Journal of the Astronautical Sciences, 52, 221

[16] Lefferts, E., Markley, F., & Shuster, M. 1982, Kalman filtering for spacecraft attitude estimation, Aerospace Sciences Meetings (American Institute of Aeronautics and Astronautics), doi:10.2514/6.1982-70

[17] Hutchinson, S., Hager, G. D., & Corke, P. I. 1996, IEEE Transactions on Robotics and Automation, 12, 651

[18] Trawny, N. & Roumeliotis, S. 2005, Indirect Kalman Filter for 3D Attitude Estimation, Technical Report 2005–002, Multiple Autonomous Robotic Systems Laboratory

[19] Diebel, J. 2006, Representing Attitude: Euler Angles, Unit Quaternions, and Rotation Vectors

[20] Steffes, S., Steinbach, J. P., & Theil, S. 2011, Investigation of the Attitude Error Vector Reference Frame in the INS EKF, ed. F. Holzapfel & S. Theil (Berlin, Heidelberg: Springer Berlin Heidelberg), 345–357

[21] Ribeiro, M. 2004, Kalman and Extended Kalman Filters: Concept, Derivation and Properties

[22] Kalman, R. 1960, Transactions of the ASME–Journal of Basic Engineering, 82, 35

[23] Shahriari, N., Fantasia, S., Flacco, F., & Oriolo, G. 2013, in 2013 IEEE/RSJ International Conference on Intelligent Robots and Systems, 77–82

[24] Havlk, J. & Straka, O. 2015, Journal of Physics: Conference Series, 659, 012022